THE ASTROPHYSICAL JOURNAL, 317:450–459, 1987 June 1

THE COMPLEX ABSORPTION SPECTRUM OF THE BROAD ABSORPTION LINE QSO 1303+308[1]

CRAIG B. FOLTZ
Multiple Mirror Telescope Observatory

RAY J. WEYMANN AND SIMON L. MORRIS
Steward Observatory, University of Arizona

AND

DAVID A. TURNSHEK
Space Telescope Science Institute
Received 1986 September 24; accepted 1986 November 20

ABSTRACT

We present spectra of the broad absorption-line QSO (BAL QSO) 1303+308, obtained with the same instrument and detector, separated in time by 2 yr. The spectra are examined for radial velocity variations of a number of the narrowest absorption components making up the broad absorption troughs. The limit on the velocity variations combined with estimates of the radiative acceleration sets a lower limit of about 3 pc on the distance of the absorbing material from the continuum source.

The spectra are also examined for temporal variations in the residual intensity of the absorption troughs. A statistically significant variation is seen in the highest (expansion) velocity absorbing material in the sense that the strength of absorption has decreased in the period between spring 1983 and spring 1985.

The BAL troughs in this object are extraordinarily complex and show interesting ordered structure. Individual C IV, Si IV, and N V doublets can be identified which are separated from other doublets of the same species by just their doublet spacing. The statistical significance of the excess number of such "line-locked" systems suggests that radiative acceleration may be important in sorting out velocities in the flow of the BAL material.

The object is also notable for its paucity of Lyman α emission. Under the assumption that this arises from absorption of the Lyman α emission by the N V broad absorption, the material responsible for the absorption must lie outside of the Lyman α broad emission-line region.

Subject heading: quasars

I. INTRODUCTION

The QSO 1303+308 (=W22722, Weistrop 1973; =PB 3296, Berger and Frigant 1977) was originally identified as a QSO by Wills and Wills (1976). In that study, the authors remark on the complex nature of the spectrum of the object, noting that the spectrum contains "broad emission lines confused by absorption features." A high-quality photographic spectrum was obtained by Weymann *et al.* (1979), who discussed the spectrum in the context of an intrinsic origin for the absorption. Weymann, Carswell, and Smith (1981) have subsequently included it in the sub-class of QSOs showing strong, often complex absorption displaced blueward from the emission-line redshift—the broad absorption-line QSOs, or BAL QSOs. In fact, of all the BAL QSOs of which we are aware, this object shows the most structure in its BAL troughs. For this reason it is of special interest as it may represent the later stages of the evolution of such objects or, in any case, is of an extreme type relative to other members of the class. Preliminary high-resolution spectroscopy was presented by Weymann and Foltz (1984) and a detailed description of the spectrum of 1303+308 was presented by Turnshek *et al.* (1984) who measured a redshift of 1.759 from the C III] emission line.

In this contribution, we present two sets of 1 Å resolution (FWHM) data covering the spectral region containing the C IV, Si IV, N V, and Lyman α emission lines and absorption troughs, separated in time by roughly 2 yr. By searching for velocity and residual intensity changes in the absorption troughs, we can attempt to refine constraints on the acceleration mechanism of the absorbing gas and /or on the distance between the continuum source and the gas responsible for the absorption.

Models for the absorption regions in BAL QSOs come in two basic varieties: (1) those in which the absorbing gas is intimately related to the gas responsible for the broad-line emission, implying a distance between the central continuum source and the absorbing gas of several to tens of parsecs and certainly less than 1 kpc, and (2) those in which the distance between the continuum source and the absorbing gas is very large compared to the size of the line-emitting region (tens to thousands of parsecs). For a detailed review of models of the absorbing regions of BAL QSOs, see Weymann, Turnshek, and Christiansen (1985).

In cases where the absorbing gas occupies a volume comparable to that of the broad-line emitting region, the absorbing material must be accelerated to velocities approaching or exceeding $0.1c$ on relatively small distance scales. The acceleration required is large enough to produce observable radial velocity variations in the absorption troughs on relatively short time scales if the acceleration is steady. For example, the acceleration, $\Delta v/\Delta t$, for the case of constant acceleration of absorbing clouds from zero velocity near the origin

[1] Observations reported here were obtained at the Multiple Mirror Telescope Observatory, a joint facility of the University of Arizona and the Smithsonian Institution.

(continuum source) to a terminal velocity of 0.1c at a distance of 10 pc is about 15 km s^{-1} month^{-1} in the rest frame of the QSO. For a $z = 2$ QSO with a broad absorption-line region (BALR) undergoing such acceleration, we would certainly expect to see a measurable radial velocity variation in the observer's frame in roughly 4 months, since we conservatively estimate that with a spectral resolution of 1 Å at 4000 Å, we can reliably detect a radial velocity variation of 30 km s^{-1}. Although the accelerations at work in the BALR are, in fact, probably considerably more complex, this simpleminded argument suggests that the search for radial velocity variations may be a fruitful one.

The only published study to date which has searched for temporal variations in the spectrum of a BAL QSO is the spectrophotometric study of PHL 5200 by Junkkarinen, Burbidge, and Smith (1983). That study presents data at roughly 10 Å resolution spanning five observing seasons (1974–1979) which exhibit no apparent changes in the residual intensities (i.e., $F_\lambda/F_{\mathrm{cont},\lambda}$, where F_λ is the observed flux in the line at wavelength λ and $F_{\mathrm{cont},\lambda}$ is the interpolated continuum flux at the same wavelength) of the C IV and Si IV absorption troughs, and no obvious radial velocity variations in any of the substructure in the trough. The latter result should not be construed as strong evidence supporting low acceleration given the low resolution of the spectra and, perhaps more importantly, the lack of prominent structure within the troughs of PHL 5200. The spectrum of 1303+308 shows the clearest structure within the absorption troughs of any known BAL QSO. The troughs in this object break up into numerous subcomponents. The remarkable structure in the absorption troughs makes 1303+308 a better candidate for monitoring temporal changes, especially $\Delta v/\Delta t$ of individual clouds, than any of the PHL 5200–type BAL QSOs.

II. OBSERVATIONS

The observations reported here were all obtained using the MMT spectrograph on the Multiple Mirror Telescope. The spectrograph was equipped with a photo-counting Reticon detector used to read out the output of a three-stage, magnetically focused ITT image tube. All observations were obtained during the springs of 1983 and 1985. No major modifications to the spectrograph or detector were made during the period between the two epochs of observation. A journal of observations is presented in Table 1. All observations were obtained in a mode where approximately 900 Å of spectral coverage are acquired in an individual integration. Observations were made at a spectral resolution slightly better than 1 Å (FWHM).

TABLE 1

1303+308 JOURNAL OF OBSERVATIONS

Date (UT)	Wavelength Coverage (Å)	Integration Time (s)
1983 Feb 13	3500–4200	4200
1983 Apr 15.....	3200–4075	4800
1983 Apr 15	3850–4600	4800
1983 May 7	3500–4050	4800
1983 May 8	3850–4600	4800
1985 Apr 19.....	3525–4425	10800
1985 Apr 20	3175–4050	3600
1985 Apr 20.....	3525–4425	3600

Data were corrected for pixel-to-pixel sensitivity variations by division by a suitably normalized quartz lamp exposure. Wavelength calibration was effected by integrations of a helium-argon lamp. More accurate calibrations were obtained after the addition of mercury and cadmium sources in 1985. Because of the dearth of strong helium and argon lines, several of the 1983 scans suffered from poor wavelength calibration shortward of about 3500 Å. We chose not to include these short wavelength regions of these scans—their omission is obvious by the limited spectral coverage reported for several observations in Table 1. Typically, seventh-order polynomials were used in the wavelength calibration procedure, and the typical standard error in the wavelength calibration fit was 0.12 Å. All spectra are reduced to heliocentric, vacuum wavelengths. In general, standard stars were not observed for this project so no attempt was made to flux-calibrate the individual scans, nor was any extinction correction applied.

Since the detector is a photon counter, the noise in the data is well understood (for the signal-to-noise ratio of the data presented here). Parallel data reduction of the variance of each pixel was carried out including the effects of photon noise in the object and sky spectra and assuming that the dark counts are Poisson distributed. Photon noise from the incandescent integrations was not included in the calculation as such noise was always negligible compared to noise from the above-mentioned sources.

The individual spectra from each observing season were then binned into a linear wavelength scale with pixels of 0.3 Å width, and co-added, weighted by their individual variances, yielding an average spectrum for each season. Prior to co-addition, each spectrum was multiplied by a constant determined by using one of the spectra as a template. No wavelength-dependent corrections were necessary. Finally, in order to illustrate the main absorption systems, the average spectra for each of the 2 yr were co-added, weighted by their individual variances, yielding the spectrum presented in Figure 1. The lower curve in Figure 1 is the 1 σ noise estimate.

Figure 1 clearly demonstrates the complexity of the structure in the BAL troughs of 1303+308. The absorbing material extends to high, though not unprecedented, ejection velocities, v_{ej}, measured relative to the emission-line redshift. We identify the redshift of the longest wavelength C IV absorption feature ($z = 1.776$) as zero velocity. (Note that this is longward of the C III] emission-line redshift quoted by Turnshek *et al.* [1984] by about 1850 km s^{-1}. This inferred "infall" velocity is uncomfortably large to be explained by the well-known tendency for redshifts derived from the centroids of the broad lines to lie blueward of the systemic redshifts. However, inspection of the data of Turnshek *et al.* [1984] shows that the C III] emission may be blended with substantial Al III λ1858 emission [cf. Hartig and Baldwin 1986] and, furthermore, the C III] redshift is considerably less than that derived from the Mg II emission.) We identify the feature denoted C IV$_{\mathrm{max}}$ as the shortest wavelength (hence, highest v_{ej}) material in the C IV absorption trough system. The redshift of the blue edge of this material is 1.545, implying an ejection velocity of about 24,000 km s^{-1}. Though this feature appears to be isolated from the remainder of the C IV BAL, the rugose nature of the continuum between this feature and the strong C IV absorption seen at lower velocity is probably due to weak C IV absorption.

In Figure 1, we indicate the positions of emission from C IV, Si IV, C II, O I, N V, and Lyman α as predicted from the C III] redshift. Note that the Lyman α emission, if present, is nearly

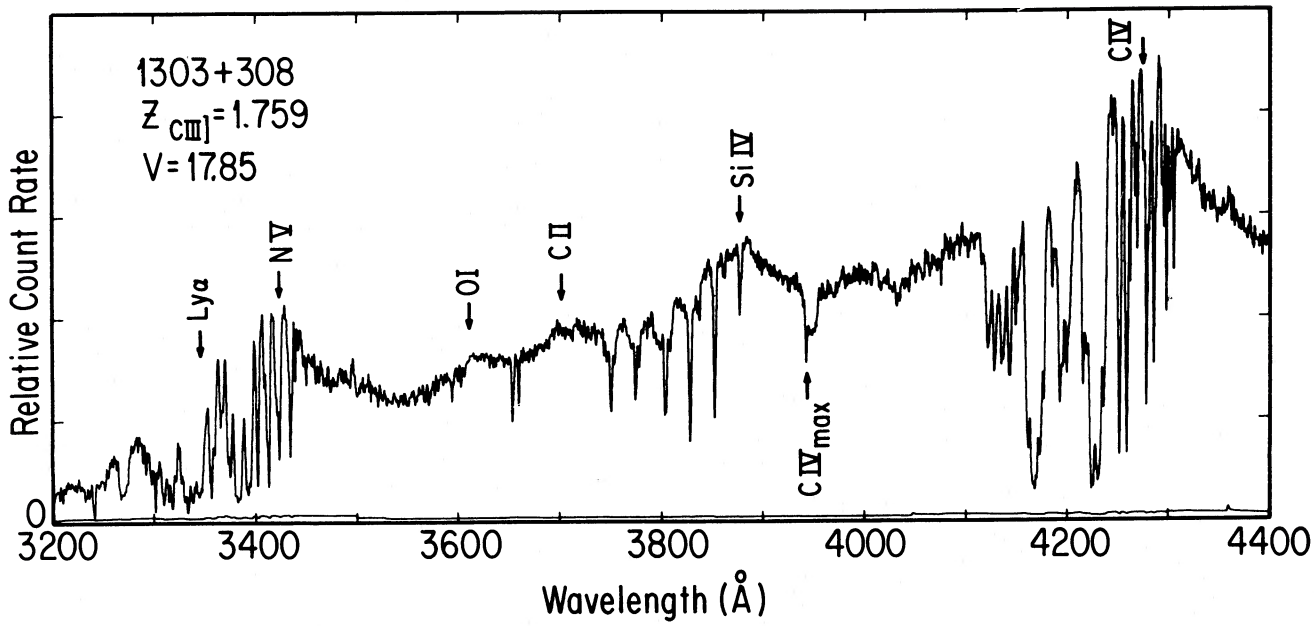

FIG. 1.—Spectrum of the QSO 1303+308 obtained with the MMT spectrograph representing the average of the data from the 1983 and 1985 observing seasons. Individual absorption features in the troughs have been marked to simplify discussion in the text. The position of strong emission lines predicted by the C III] λ1909 redshift of 1.759 have also been marked. The curve at the bottom of the figure shows the 1 σ error level as derived from counting error in the object and sky spectra. Discontinuities in the noise spectrum show the limits of individual spectra.

completely obliterated by the N V + Lyman α absorption troughs, providing additional evidence that the material responsible for the broad absorption is outside the emitting region responsible for the Lyman α emission. It is possible that the broad Lyman α emission is intrinsically weak in this object, as it appears to be in the case of the BAL QSO 1309−056. However, the Mg II emission line, which is presumably produced in a region of high Lyman α emissivity, is not anomolously weak (Turnshek *et al.* 1984).

The spectrum exhibits no strong evidence for a component of Lyman α emission from a narrow-line emitting region (NELR). This could be due to the lack of a NELR, or the absorbing material could be occulting any narrow-line emission. We attempt to set an upper limit on the amount of narrow Lyman α emission as follows: In Figure 2, we present an expanded plot of the region containing the N V BAL and the predicted position of the Lyman α emission. The indicated position of Lyman α may be in error due to well-known systematic differences between the redshift of broad, high-ionization lines and the QSO's systemic redshift (which would presumably be close to the redshift of Lyman α emission from the NELR). The solid line is a linear extrapolation of the continuum longward of the N V emission line. For the sake of deriving an upper limit on the amount of narrow Lyman α emission, we liberally assume that all of the continuum and broad Lyman α are eradicated by the N V BAL and that all of the shaded area in the figure (±2000 km s^{-1} of the predicted position) is due to narrow Lyman α emission. Referred to the interpolated continuum, the equivalent width of all of the dashed region is 42 Å. Therefore, either the narrow Lyman α emission is absorbed by the BAL (which implies that the size of the BALR is even bigger than that of the narrow emission-line region) or the rest equivalent width of such emission is less than about 15 Å. It is worth noting that most high redshift QSOs of luminosity comparable to 1303+308 do not have significant Lyman α emission.

We also note the difference between the appearance of the C IV and Si IV troughs. The equivalent width of the C IV trough is much larger than that of the Si IV trough and the Si IV absorption is much simpler than that of C IV in the sense that there are a few strong doublets which seem to be accompanied by weaker features. The region containing the Si IV trough is presented in Figure 3. In this figure we indicate the position of six relatively narrow (though not unresolved) doublets. These features are real in the sense that both members of each doublet has an equivalent width greater than 5 times its uncertainty as derived from the spectrum of the variances. Wavelengths, and *observed* equivalent widths for these strong features are presented in Table 2. In all cases, the uncertainty in the observed equivalent width is slightly less than 50 mÅ. In constructing this table we have attempted to identify only the relatively unblended components. There is certainly weak absorption present which we cannot resolve or which is intrinsically blended. Table 2 also presents the ratios of the equivalent widths of the members of the doublet, $W(\lambda 1393.76)/W(\lambda 1402.77)$, and the ratios of the observed wavelengths of the members of each doublet.

Two of the strong Si IV doublets, *C* and *F*, are separated by just the doublet spacing. Furthermore, the ratio of their equivalent widths can only be explained if an additional system, doublet *D*, is present such that the long wavelength member of *C* is coincident with the short wavelength member of *D* and the long wavelength member of *D* is coincident with the short wavelength member of *F*. The ratios of the wavelengths of the members of the Si IV doublet is invariant with redshift, having a value of 1.00647. Adopting 0.3 Å a conservative estimate of the uncertainty in measuring the centroids of these features, we find ratios of 1.00643, 1.00638, and 1.00649 ± 0.00010 for

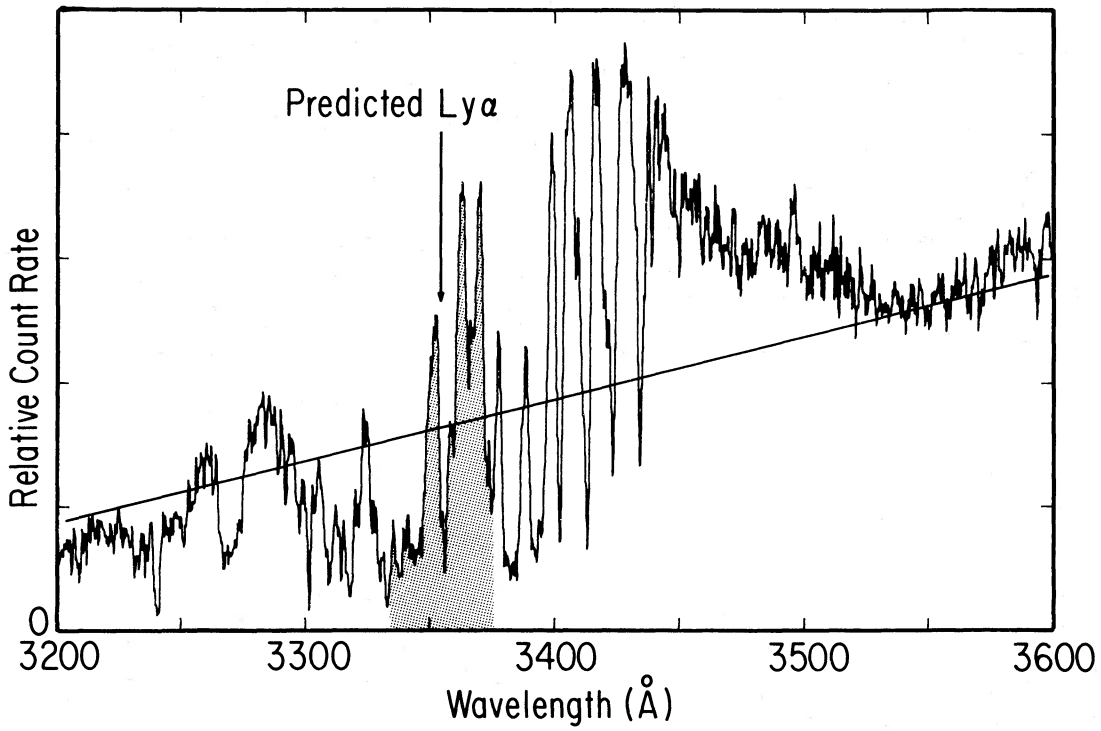

FIG. 2.—The region of the spectrum presented in Fig. 1 containing the predicted position of Lyman α emission. The solid line is an extrapolation of the continuum from longer wavelengths. If the shaded area were due to Lyman α emission, then it would have a rest equivalent width (referred to the interpolated continuum) of 15 Å.

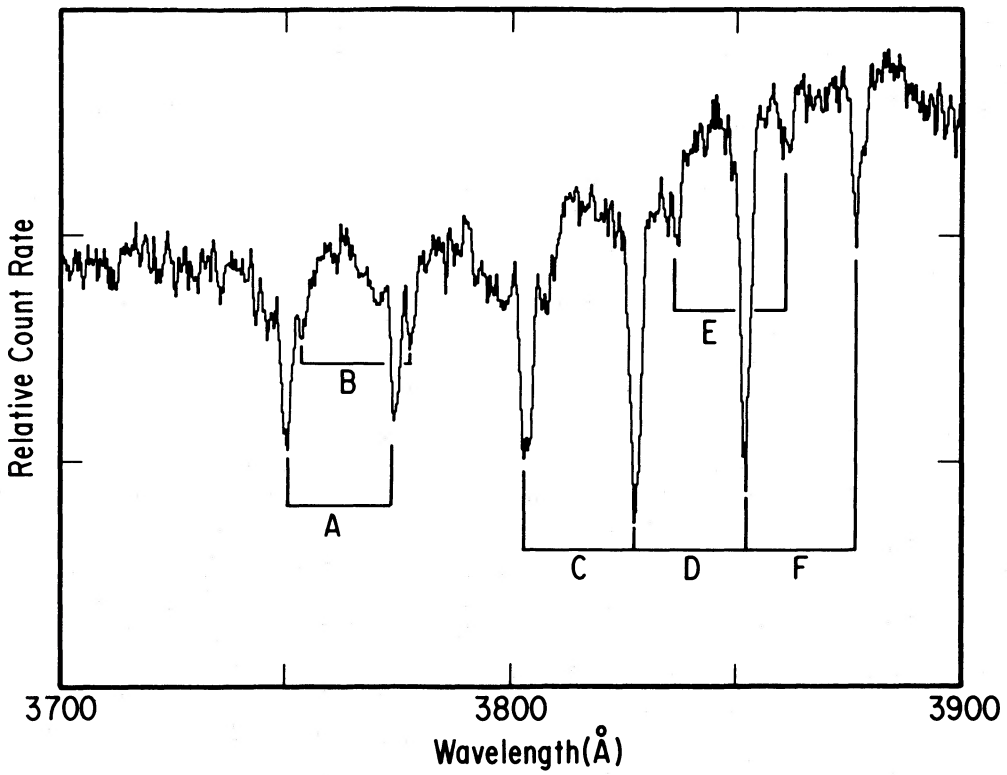

FIG. 3.—The region of the spectrum presented in Fig. 1 containing the Si IV absorption trough. The minimum number of systems needed to explain the strong, narrow components is six. The positions of individual systems are marked. Note that system *D* is "locked" to systems *C* and *F*.

TABLE 2

Si IV λλ1393.755, 1402.770 DOUBLETS

System	λ_{obs} (Å)	W_{obs} (Å)	$W(\lambda1393)/W(\lambda1403)$[a]	$\lambda_{1393}/\lambda_{1403}$[b]
A.....	3749.85	1.20	1.24 ± 0.08	1.00646 ± 0.00010
	3774.06	0.97		
B.....	3753.12	0.44	0.98 ± 0.15	1.00647 ± 0.00010
	3777.42	0.45		
C.....	3802.95	1.70	0.84 ± 0.03	1.00643 ± 0.00010
	3827.39	2.03		
D.....	3827.39	2.03	1.25 ± 0.05	1.00638 ± 0.00010
	3851.79	1.62		
E.....	3835.95	0.30	1.36 ± 0.38	1.00644 ± 0.00010
	3860.65	0.22		
F.....	3851.79	1.62	2.66 ± 0.23	1.00649 ± 0.00010
	3876.77	0.61		

[a] Uncertainties derived assuming $\sigma_w = 0.050$ Å. Actual value should lie in the range between 1.0 for saturated lines and 2.0 for unsaturated lines.

[b] Uncertainties derived assuming $\sigma_\lambda = 0.3$ Å. Actual value for this ratio is 1.00647.

systems *C*, *D*, and *F*, respectively. Therefore, to account for the wavelengths and strengths of the features, the middle doublet must be "locked" to doublets *C* and *F*. Confirmation of the reality of system *D* is provided by identification of both members of the C IV and N V doublets at the same redshift. Other examples of this phenomenon can be found in the C IV and N V troughs. We comment on the statistical and physical significance of this "line-locking" in § IV, below.

Finally, we note that the ionization of the material in the absorbing regions is fairly typical, based upon the species that are available for study in our limited wavelength range. There is apparently no C II λ1334 absorption. Our 3 σ upper limit on the observed equivalent width of a 3 Å wide feature in the region shortward of the C II emission line is 135 mÅ at the positions corresponding to the strongest Si IV and C IV components. We assume here that any C II absorption would be fairly sharp—we cannot rule out the possibility of a smooth, weak C II trough, though such a smooth trough may be unexpected given the complexity of the other absorption troughs. Though we cannot rule out the possibility of any Lyman α absorption, the observed absorption in the spectral region shortward of N V emission can be explained solely by N V absorption given the range of v_{ej} observed in the C IV trough. There are no very strong features corresponding to Lyman absorption at the redshift of strong C IV components.

III. SEARCH FOR TEMPORAL VARIATIONS

The two issues which these data are used to address are (*a*) temporal variations of the residual intensities of the absorption troughs, and (*b*) the possible existence of temporal variations in the radial velocity of the absorption troughs. Variations of the first kind might be expected for a variety of reasons: e.g., the column densities of the clouds may be changing due to expansion or evaporation of the clouds, or the ionization level in the clouds changing due to changes in the output of the ionizing source. Variations of radial velocity give a measure of the cloud acceleration. Though the 1983 data set was obtained during a period spanning 3 months, the mean time difference between the two data sets was almost exactly 2 yr. Therefore, in the rest frame of a $z = 1.759$ QSO, this elapsed time is 24 months/(1 + *z*), or about 8.7 months.

a) Residual Intensity Variations

Residual intensity variations in the C IV trough, if any, are subtle. In order to demonstrate the similarity of the two spectra, we reproduce redward parts of the C IV troughs of the individual spectra in Figure 4. After experimenting with a variety of overplotting techniques, we decided that the best way to compare the two spectra is for the reader to duplicate one of the panels of Figure 4 onto a transparency and lay it on top of the other panel. Note the decrease in the residual intensity of the components of C IV absorption at about 4130 Å. The formal significance of these differences can be determined by integrating the corresponding wavelength region in the difference spectrum and its associated variance spectrum. The departure from zero of the sum of the difference spectrum over the wavelength range 4113–4155 Å is 4.2 σ. In Figure 5 we show the Si IV BALs and the blueward parts of the C IV BALs. Inspection of this figure shows that while none of the strong Si IV components exhibit strong residual intensity variations, there is a suggestion that some of the weaker components have decreased in strength during the epoch between two observations. Furthermore, a real decrease in the strength of the highest velocity C IV components is seen. Integrating the difference spectrum and its associated variance spectrum over the wavelength range 3940–3955 Å indicates that the significance of the decrease in the equivalent width of the feature is significant at the 6 σ level.

b) Radial Velocity Variations

With the exception of several of the sharp, low-velocity components of the C IV trough and the strong narrow Si IV features, it is difficult to measure the centroid of the absorption troughs accurately due to the widths of the troughs. Since these narrow features are not distributed over the entire velocity range of the absorption troughs, we do not get an estimate of the acceleration as a function of ejection velocity. To circumvent this problem and to attempt to derive an objective estimate of the velocity variation (or limit thereon) we chose the following procedure. First we constructed the difference between the two spectra in the sense 1985 data − 1983 data. Since the spectra were all shifted to a constant level before co-addition, this difference averaged zero in the regions outside of the absorption troughs. This spectrum was then divided by the spectrum of the expected uncertainties (the square root of the sum of the squares of the variance spectra) on a pixel-by-pixel basis. The resulting spectrum of differences normalized to the number of σ deviation is plotted in panel (*a*) of Figure 6 for the redward part the C IV trough. Examination of this spectrum shows no significant (> 4 σ) deviations from zero in a sample of 820 pixels. In order to evaluate what this lack of significant deviations implies in terms of the minimum detectable velocity variation, we then repeated the calculation after shifting the 1983 data to the red by 15, 30, and 45 km s^{-1}. The results are shown in panels (*b*), (*c*), and (*d*) of Figure 6, respectively. Comparison of these panels with the real difference spectrum (panel [*a*]) allows the following statements to be made: The presence of the narrow components at low apparent ejection velocity allows us to set an upper limit of less than about 15 km s^{-1} on the radial velocity variations for v_{ej} < about 2000 km s^{-1}. At higher velocities, the limits are higher due to the lack of narrow features, though we feel that reasonable limits on Δ*v* are 30 km s^{-1} at v_{ej} = 5000 km s^{-1} and 45 km s^{-1} at v_{ej} = 10,000 km s^{-1}. The results at the highest ejection velocities are made

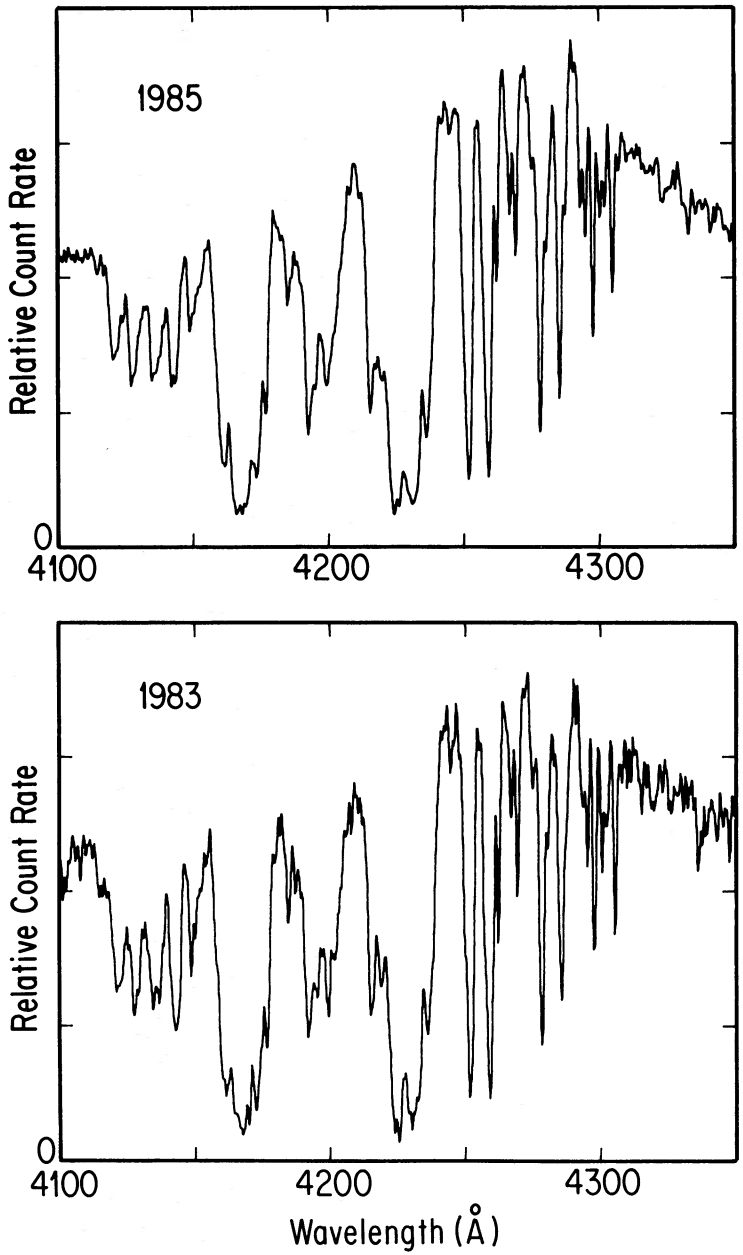

FIG. 4

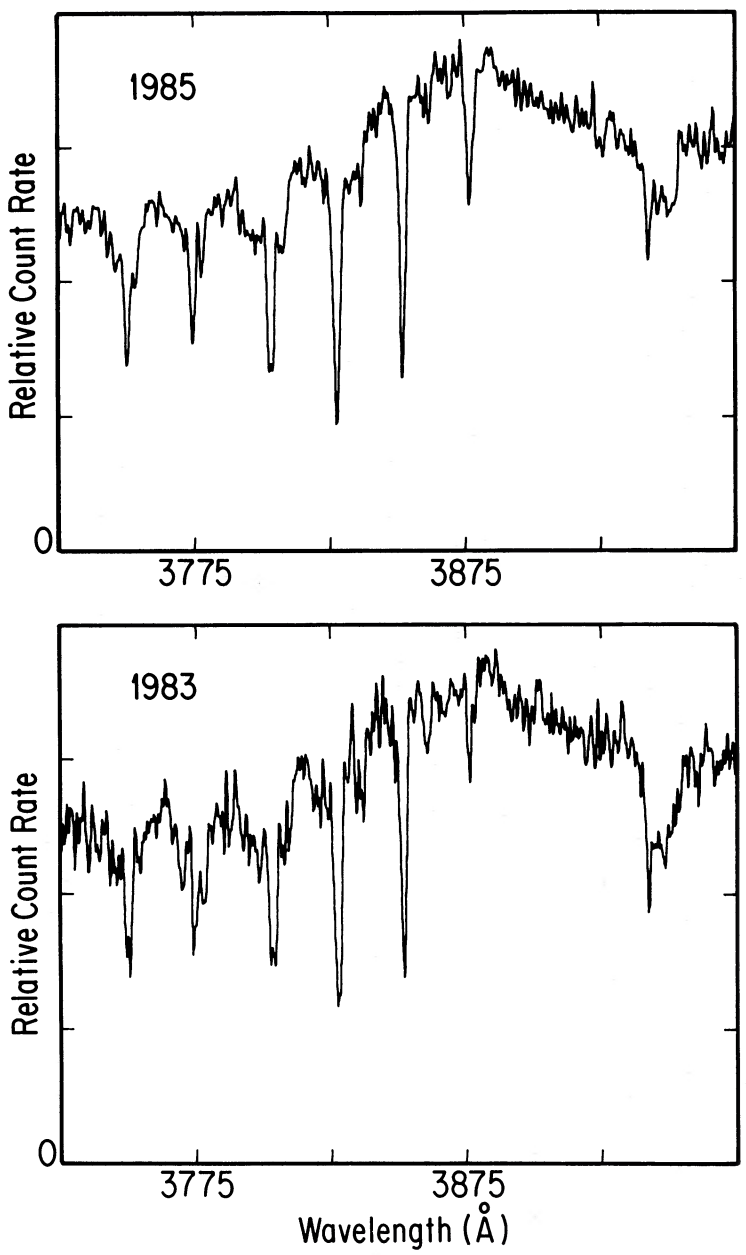

FIG. 5

FIG. 4.—Spectra of 1303+308 in the region containing the redward parts of the C IV broad absorption trough obtained in 1983 (*top*) and 1985 (*bottom*). The similarity between the two spectra can be demonstrated by reproducing one of the spectra onto a transparency via a xerographic process and overlaying the two spectra.

FIG. 5.—As in Fig. 4 for the Si IV BALs and the blueward part of the C IV BAL. Note the apparent change in the highest velocity (bluest) component of the C IV BAL.

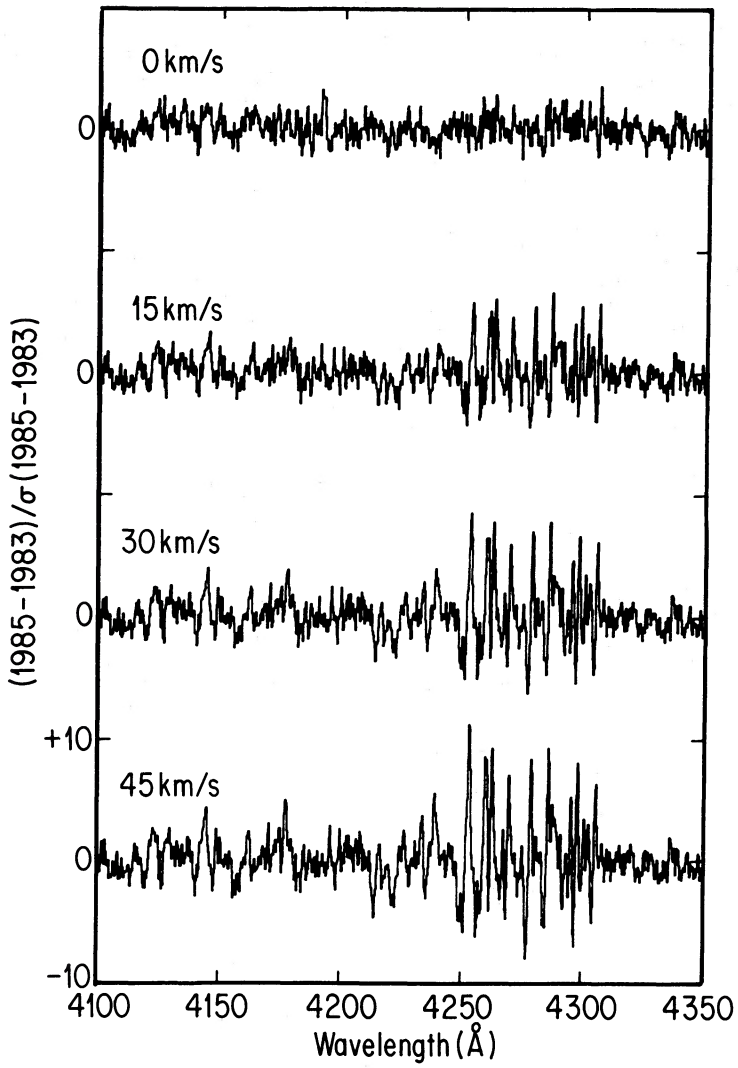

FIG. 6.—(*a*). The difference between the spectrum obtained in 1985 and that obtained in 1983 (in the sense 1985 minus 1983) divided by the square root of the sum of the variances of the two spectra. (*b*). As in (*a*) except that the 1983 data have been shifted redward by 15 km s^{-1}. (*c*). As in (*b*) with a shift of 30 km s^{-1}. (*d*). As in (*b*) with a shift of 45 km s^{-1}.

somewhat ambiguous due to possible residual intensity variations. The results are independent of whether the 1983 data are shifted to the red or blue before subtracting from the 1985 data. Similar limits result from applying the same procedure to the Si IV region.

IV. DISCUSSION

a) Line Locking

There has been considerable discussion on the subject of line locking in the QSO literature during the early to middle 1970s (e.g., Scargle 1973; Strittmatter *et al.* 1973; Burbidge and Burbidge 1975; and Sargent and Boroson 1977). These papers were generally discussing absorption line systems in non-BAL QSOs. The conclusion reached by the last of these papers is that there is little or no evidence for line locking in this class of object. This conclusion added support to the intervening hypothesis for the location of the absorbing clouds.

The question that we need to address here is whether line locking is present in the absorption spectrum of a BAL QSO, that is, in an object in which the absorbing material *is* thought to be ejected by the QSO, and will thus be subject to a non-isotropic radiation field.

In § II we presented evidence for line locking between individual components within the BAL troughs. The cleanest statistical test of the reality of this phenomenon is provided by the Si IV lines, since the lines are rather sharp, the continuum well-defined, and the crowding not severe. If we apply the standard analysis to detect the presence of absorption lines (see, for example, Foltz *et al.* 1986) and accept, as in that paper, only systems in which both members of the doublet have a formal significance of 5 σ or greater, then there are only six systems, i.e., those listed in Table 2.

The striking feature of the Si IV region is the series of four lines at wavelengths 3802.95, 3827.39, 3851.79, and 3876.77 Å which comprise the three doublet systems *C*, *D*, and *F*, where system *D* is locked to the other two systems. The reality of system *D* is fairly secure in that (i) the ratio of the wavelengths of the two members of the doublet is 1.00638 ± 0.00010 as compared to the value for the Si IV doublet of 1.00647; (ii) the

doublet ratios for systems *C* and *F* lie outside of the range 1–2, implying additional absorption must be present; and (iii) features are present in both the C IV and N V troughs which can be identified as absorption at the redshift of system *D*.

We now estimate the likelihood of this case of apparent double line locking occurring by chance, assuming that six systems are distributed randomly over some range of velocities. (This is a different calculation than the probability of two separate cases of "single" locking involving four of the six systems.) We assume that locking would apparently be present if the red member of one system lies within the FWHM line width of the position of the blue member of another system. (This is a conservative assumption in terms of the probability reported below since the three doublets under consideration are locked to a tighter tolerance than this—the total velocity spread between the short wavelength member of system *C* and the long wavelength member of system *F* is 5770 km s^{-1}, as compared to 3 times the doublet spacing = 5780 km s^{-1}.) We measure the average FWHM of the unlocked strong components to be 200 km s^{-1}. While it is not obvious to us what to select as the range of velocities over which the systems could have been distributed, it is easy to show that if six systems are distributed randomly over some region, then the expected ratio of the difference in velocity between the reddest and bluest of the six systems to the full velocity range is $\frac{5}{7}$. Therefore, since the six observed doublets span 8050 km s^{-1}, we adopt 11,300 km s^{-1} as the region over which we will cast randomly distributed Si IV doublets. A straightforward calculation then yields the result that the probability of occurrence a double line lock for six randomly distributed doublets is about 0.02. If we halve the wavelength tolerance for an assumed lock and require that in order for two systems to be locked, wavelength coincidence must be within ± 50 km s^{-1}, this probability drops to about 0.006. This admittedly *a posteriori* treatment suggests to us that "fine-tuning" of the dynamics of the clouds in this object by radiative acceleration really is operating.

Analysis of the entire set of systems including those represented by the C IV and N V lines is far more ambiguous due to the complexity and degree of blending in the C IV and N V troughs. However, examples of line locking can be found in both—a clear case can be seen at the red edge of the N V trough shown in Figure 2 where four relatively narrow features are separated from each other by the N V doublet spacing.

There has been little detailed modeling of line locking in the literature, but some simple conclusions can be drawn if line locking is present in 1303+308.

1. Radiation pressure resulting from absorption by the resonance lines of C IV, Si IV, and N V must be a significant perturbation to the net force on the absorbing clouds.

2. The net acceleration of the more distant clouds ($\dot{v}_d$) must be greater than the acceleration of the nearer clouds ($\dot{v}_n$), i.e., $\dot{v}_d > \dot{v}_n$.

For example, a plausible scenario satisfying the above constraints would be radiatively driven clouds, subject to a drag force falls off more rapidly than $1/r^2$.

It should be mentioned that line locking in SS 433 was recently modeled in considerable detail by Shapiro, Milgrom, and Rees (1986). However, their study considered only locking between a hydrogenic ion's Lyman α line and the hydrogen Lyman edge, and as the continuum source in 1303+308 is not expected to have any such edge, their models are unlikely to be relevant.

b) *Some Inferences on the Location and Properties of the Clouds*

From the limits that have been set on the acceleration in the previous section, we may make some crude estimates of the distances of the clouds from the central source. We consider two possible approaches for such estimates.

1. Limits on the distances assuming that radiative acceleration is the only force acting on the clouds (e.g., there is no drag): We use the expression given by Weymann, Turnshek, and Christiansen (1984) which assumes that the individual clouds are optically thin to the main resonance lines. Then the acceleration is given by

$$a = \frac{L_\nu}{4\pi r^2 c}\left(\frac{\pi e^2}{mc}\right)\sum_i f_i\left(\frac{n_i}{\rho}\right), \quad (1)$$

where L_ν is the estimated monochromatic luminosity, and the sum is over the lines of C IV, Si IV, N V, and O VI, with the estimates for fractional ionizations from Weymann, Turnshek, and Christiansen (1984). For the limits on the acceleration quoted in § III, we then find from equation (1) that the low-velocity clouds must be at distances greater than 5 pc, while the high-velocity clouds must be at distances of greater than 3 pc. These distances are sufficiently large that models of the type described by Drew and Boksenberg (1984) are probably not applicable to this object.

2. Limits on the distance assuming acceleration by a wind: We envision the clouds being accelerated by the ram-pressure of a thermal wind, such as that described by Weymann *et al.* (1982). In that paper, the trajectory of a cloud embedded in such a wind was computed. (Cf. Fig. 2 of Weymann *et al.* 1982.) We assume that the clouds in 1303+308 follow similar trajectories in the following sense: We define a dimensionless distance

$$x = r/R_{\rm sonic}$$

and a dimensionless velocity

$$w = v/V_{\rm terminal}\,.$$

We further assume that the function $w(x)$ is the same function in 1303+308 as it is for the case of Figure 2 of Weymann *et al.* (1982) (for which the cloud trajectory has a terminal velocity of approximately 25,000 km s^{-1} and a sonic point radius of approximately 0.53 pc). Then the following inequality holds:

$$r = xR_{\rm sonic} > xV^2_{\rm terminal}\,q/a_{\rm lim}\,, \quad (2)$$

where

$$q = \frac{w^2}{x}\frac{d\log w}{d\log x} \quad (3)$$

is taken from Figure 2 of Weymann *et al.* (1982), $a_{\rm lim}$ is the (velocity dependent) limit on the acceleration discussed in § III, and the radii and velocities in equation (2) refer to those in 1303+308. We adopt a value of $V_{\rm terminal} = 24{,}000$ km s^{-1} for 1303+308 on the grounds that the highest velocity cloudlets we can see in the C IV lines have velocities a little less than this. For each observed cloud velocity, v, we thus compute the corresponding dimensionless velocity w. From Figure 2 of Weymann *et al.* (1982), we may then compute x, as well as the dimensionless acceleration parameter q. Finally, associating a value for the upper limit on the acceleration of the clouds for

TABLE 3

LOWER LIMITS ON THE CLOUD DISTANCE

V (km s^{-1})	$a_{\rm lim}$ (cm s^{-2})	w	x	q	$R_{\rm lower\ lim}$ (pc)
2000.....	0.066	0.083	0.28	0.028	0.0015
5000.....	0.131	0.208	0.97	0.032	0.019
10000.....	0.197	0.42	3.77	0.021	0.13

that velocity yields, via equation (2), a lower limit for the distance of the cloud from the source. The results for a few representative velocities are shown in Table 3.

Clearly these limits are rather strongly model-dependent and not terribly interesting. In particular, as shown in § IV*a*, "radiative line locking" is probably operating as well, and this certainly complicates the discussion of limits on the distances of the clouds from the source of radiation.

The best *upper limits* on the distance of the BALR from the continuum source are derived from observations of the lack of broad [O III] $\lambda\lambda$4959, 5007 emission in the two low-redshift BAL QSOs PG 1700+518 (Turnshek *et al.* 1985) and PG 1416−129 (Turnshek and Grillmair 1986). In these two QSOs the derived upper limit on the BALR-continuum separation is about 50 pc. This limit scales as the square root of the continuum luminosity. Therefore, if 1303+308 also exhibits no broad [O III] emission at the same level as in these QSOs, we could infer an upper limit on this distance of about 200 pc.

We have also presented evidence in § III that the strength of the weaker absorption features at high velocities has decreased with time over the period covered by our observations. This could be due to a number of causes including:

1. Changes in the ionization of the clouds due to changes in the strength of the continuum source. If this is the case, then the continuum variations should be almost exactly in phase with the variations in line strength, since the recombination and ionization time scales are probably very short. We have begun a program of photoelectric monitoring of the source to check this.

2. The clouds are undergoing evaporation by surrounding hot gas. We can think of no way to check this possibility, nor can we easily associate any characteristic cloud property with this time scale since the evaporation process may be very complex.

3. The clouds, since being formed, are simply "thinning out." If they move into regions of lower pressure, if they are pressure-confined, if the clouds have constant mass and expand homologously, if the density of the confining gas drops as $1/r^2$ (as it would for spherically symmetric steady flow at constant velocity), if the confining gas is nonrelativistic and expanding adiabatically, if the gas in the clouds behaves isothermally, and finally, if we ignore ionization changes associated with the changing density in the cloud (since for C IV we are probably near the maximum in the C IV ionization fraction), then one can show that the C IV column density changes is related to the change in distance from the source by

$$\frac{\Delta N}{N} \approx \frac{-20}{9}\frac{\Delta R}{R}. \quad (4)$$

Taking the relative change in the column density to be about 0.20 implies that $\Delta R/R$ is about 0.1. Setting $\Delta R = v\Delta t$ leads to the rather uninteresting and improbable value of $R \approx 0.07$ pc. This, together with the long concatenation of "ifs" listed above, leads us to think that other processes besides "thinning out" are at work in changing the column density of the clouds.

V. SUMMARY

We present spectra of the BAL QSO 1303+308 obtained 8.7 months apart in the rest frame of the QSO. The spectra exhibit clear structure in the absorption troughs which, in itself, provides strong evidence for a "clumpy" nature for the BALR. The lack of Lyman α emission implies that the BALR is larger than the Lyman α emitting region. Furthermore, the rest equivalent width of any narrow Lyman α emission is less than about 15 Å.

The strength of the absorption appears to have decreased slightly in the highest velocity C IV components. Changes are not apparent in any other ion.

The lack of radial velocity variations between the two epochs of observation allows us to set a limit on the observed acceleration of less than about 1.7 km s^{-1} month^{-1} in the frame of the QSO. Limits on the acceleration as a function of recessional velocity for the clouds, together with some model dependant assumptions, allow us to set lower limits on the QSO-cloud distance (for the high-velocity clouds) of >3 pc for radiatively accelerated clouds and >0.13 pc for clouds embedded in a wind.

We find examples of absorption systems which are separated in velocity from their neighboring systems by just the velocity separation of the members of the appropriate doublet. The clearest examples of this phenomenon are visible in Si IV, but examples are also seen in the C IV and N V troughs. We interpret this to imply that radiation pressure is a significant perturbation in the BAL cloud dynamics.

We express our gratitude to Dr. F. H. Chaffee, Jr., the Director of the Multiple Mirror Telescope Observatory, for making available some of the observing time used during the spring 1985 observations. We also wish to thank C. Heller, J. McAfee, and J. Robertson for their cheerful assistance at the MMT. This research was supported, in part, by the National Science Foundation under grants AST 81-09025 and AST 83-03766 to the University of Arizona. S. L. M. acknowledges the support of S.E.R.C. and Lindemann fellowships and the hospitality of the Steward Observatory.

REFERENCES

Berger, J., and Frigant, A. 1977, *Astr. Ap. Suppl.*, **28**, 123.
Burbidge, E. M., and Burbidge, G. R. 1975, *Ap. J.*, **202**, 287.
Drew, J., and Boksenberg, A. 1984, *M.N.R.A.S.*, **211**, 813.
Foltz, C. B., Weymann, R. J., Peterson, B. M., Sun, L., Malkan, M., and Chaffee, Jr., F. H. 1986, *Ap. J.*, **307**, 504.
Hartig, C. F., and Baldwin, J. A. 1986, *Ap. J.*, **302**, 64.
Junkkarinen, V. T., Burbidge, E. M., and Smith, H. E. 1983, *Ap. J.*, **265**, 51.
Sargent, W. L. W., and Boroson, T. A. 1977, *Ap. J.*, **212**, 383.
Scargle, J. D. 1973, *Ap. J.*, **179**, 705.
Shapiro, P. R., Milgrom, M., and Rees, M. J. 1986, *Ap. J. Suppl.*, **60**, 393.
Strittmatter, P. A., Carswell, R. F., Burbidge, E. M., Hazard, C., Baldwin, J. A., Robinson, L., and Wampler, E. J. 1973, *Ap. J.*, **183**, 767.
Turnshek, D. A., Foltz, C. B., Weymann, R. J., Lupie, O. L., McMahon, R. G., and Peterson, B. M. 1985, *Ap. J. (Letters)*, **294**, L1.
Turnshek, D. A., Weymann, R. J., Carswell, R. F., and Smith, M. G. 1984, *Ap. J.*, **277**, 51.
Turnshek, D. A., and Grillmair, C. J. 1986, *Ap. J. (Letters)*, **310**, L1.
Weistrop, D. 1973, *Astr. Ap.*, **23**, 215.
Weymann, R. J., Carswell, R. F., and Smith, M. G. 1981, *Ann. Rev. Astr. Ap.*, **19**, 41.

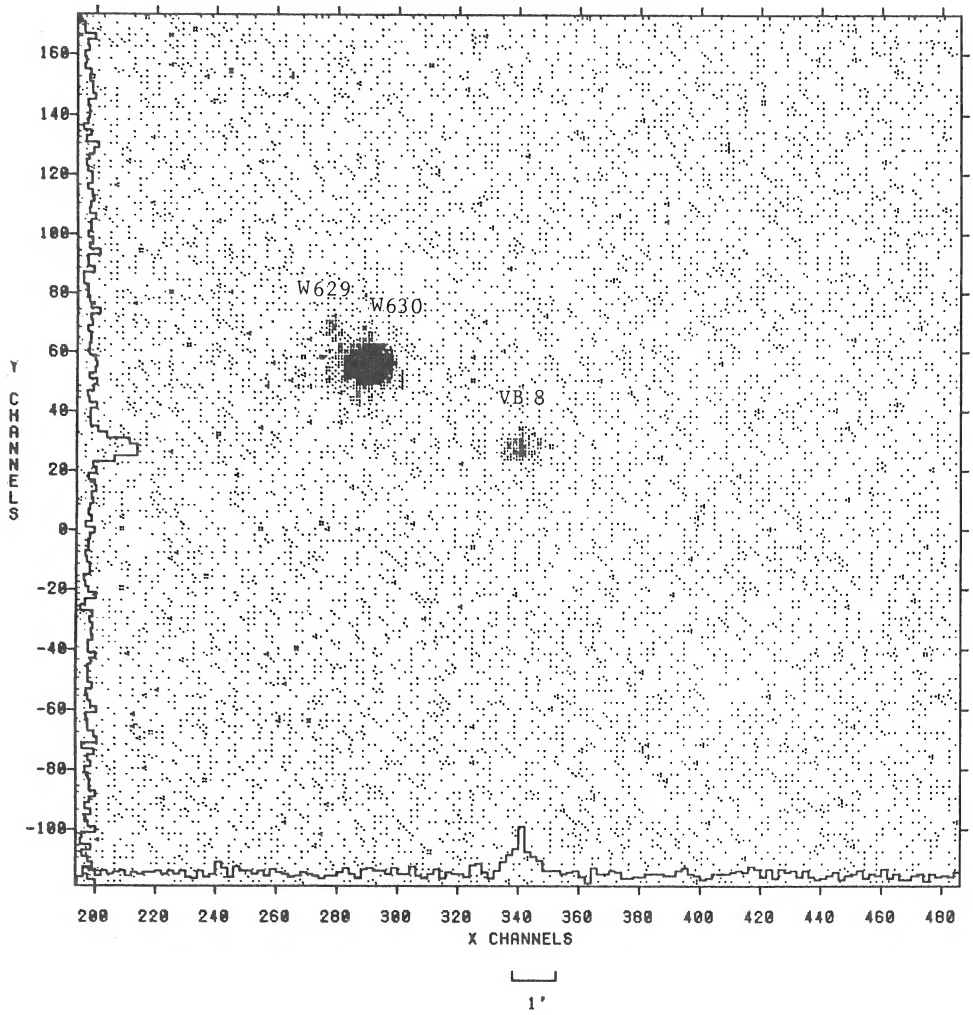

FIG. 1.—Full-resolution image of the Wolf 630 system made with the *EXOSAT* low-energy telescope. North is 174° from the positive *X*-axis. The histograms show the relative count rates in strips of *X* and *Y* channels that include the image of VB 8.

images, and background counts in an annulus from 64″ to 184″; but the image of W629 required source counts in a radius of 21″ so as not to encompass the image of W630, and the background count rate of W630 in the reduced area was applied to W629. Table 1 also lists HRI data specially reprocessed with global background instead of DETECT background, which is too high for W629 and VB 8 in proximity to W630 (cf. *Einstein Observatory Revised User's Manual* 1984).

Table 1 quotes the W630 dominant plasma temperature T measured with the SSS. This value of T was used in one of a series of isothermal plasma models (Raymond and Smith 1977) updated by Raymond (1986), with absorption by interstellar $N_H = 1E18$ cm^{-2}, and folded through the response functions of the *EXOSAT* and *Einstein* instruments. In accordance with the SSS result, a low Fe abundance (0.6 of solar) is put into the models. The model ratio of CMA to HRI count rates for W630 at $T = 6.5E6$ K exceeds the observed ratio by 12%. The difference of ratios may be a result of change of X-ray flux between dates of the observations. The difference of ratios could be reduced by assuming a slightly higher T in the model; higher N_H would also work, but the relative telescope efficiencies may not be known to better accuracy than the accuracy of these parameters.

The observed ratio of CMA to HRI count rates for VB 8 (increased by 12% in accordance with the preceding remarks) generally yields two values of model T(HRI) for any value of model T(CMA), but the assumption of equal T for the two observations has the single solution, $T = 6.4E5$ K, as given with errors in Table 1. The quantity T should be higher in a flaring state than in a quiescent state, so that the flare observed with the CMA should make T(CMA) > T(HRI), which acceptably leaves the lower value of a quiescent T(HRI) < 6.4E5 K. The observations interpreted with the models thus lead to $T \leq 6.4E5$ K for the quiescent corona of VB 8, and $T \geq 6.4E5$ K for its flaring state, where $T \approx 6.4E5$ holds if the corona was equally active during both the HRI and the CMA observations.

Tabulated emission measure for the dominant coronal plasma of W630 is from Swank and Johnson (1982), and emission measure for VB 8 is from the HRI functions illustrated by